NANOFLUID POOL BOILING AND DEPOSITION ON A CYLINDER

Mahdavi M., Sharifpur M. and Meyer J.P.
Department of Mechanical and Aeronautical Engineering,
University of Pretoria,
Pretoria, 0002,
South Africa,
E-mail: mohsen.sharifpur@up.ac.za

ABSTRACT

There are still some unknown aspects of nanofluids regarding simulations. Pool boiling flows are complicated in terms of numerical modelling and presence of particles can noticeably expand this complexity. Two-dimensional pool boiling flow with nanoparticles is numerically solved around a horizontal cylinder for validation purposes. For further study, a tube bundle with four tubes is considered with nanofluid pool boiling. Unsteady Eulerian two-fluid model in ANSYS-Fluent is used to simulate the liquid and vapour flows in the computational domain. On the other hand, the particles are injected and tracked in the domain in the Lagrangian frame via the discrete model. Coupling between two frames is carried out through some user defined functions and the effects of final outcomes appear as thermos-physical properties. It means that nanofluid mixture properties are a function of local volume fraction. Superheat temperature and heat transfer coefficient from modelling are compared with experimental measurements. The good agreement is found and further discussion regarding particles migration and deposition are presented. Since the real fluctuation of the surface roughness cannot be introduced, an estimation of deposition predicted by the discrete model is presented. It is found that the percentage of deposition depend on heat flux and a weak function of particle concentration.

INTRODUCTION

Dilution of liquids via fine solid particles can result in heat transfer enhancement in heat exchangers and other industrial equipment. This is somehow referred to improvement in thermal conductivity of the mixture [1, 2]. On the other hand, since the increase in mixture viscosity is inevitable, improvement or deterioration of final thermal efficiency can be still in doubt, reported in some experimental measurements [3, 4]. Due to the extensive area of applications, nanofluid can be used in both single and multiphase flows. Laminar and turbulent forced convection in pipes and heat exchangers are some of the common examples in single phase flows [5, 6]. On the multiphase perspective, using fine particles in boiling flows has attracted great attention in recent years [7], with the particular application in pressurized and boiling reactors. Experimental observations show both enhancement and worsening of heat transfer coefficient using nanoparticles, depending on the type and size of the particles, type of the stabilizer, base fluid and flow, geometry and surface roughness [8]. Due to the complexity and many phenomena involved in pool boiling flows, especially with the presence of solid particles, the number of numerical work is limited and most of the previous studies cover experimental measurements and visualization.

NOMENCLATURE

A_i	[m^2]	interfacial area
A_p	[m^2]	particle projected area
C_L		lift coefficient
C_w		wall lubrication coefficient
C_c		cunningham correction factor
C_D		drag coefficient
C_{ML}		rotational coefficient
C_ω		rotational drag coefficient
C_{qw}		bubble waiting time coefficient
c_p	[J/kg.K]	specific heat
d	[m]	diameter
d_p	[m]	particle diameter
d_w	[m]	bubble departure diameter
D_T	[m^2/s]	thermophoresis diffusion coefficient
h	[W/m^2.K]	heat transfer coefficient
h_k	[J/kg]	enthalpy
h_{lv}	[J/kg]	latent heat of evaporation
k	[W/m.K]	Thermal conductivity
K_B	[m^2.kg/^{o}K.s^2]	Boltzmann constant
m_p	[kg]	particle mass
M_k	[kg/m^2.s^2]	momentum induced by mass exchanged
N_w		nucleate site density
Nu		Nusselt number
n_w		wall normal vector
Pr		Prandtl number
q_k , q_k^t	[W/m^2]	laminar and turbulent heat flux
Re		Reynolds number
Re_p		particle Reynolds number
Re_{ω_p}		angular Reynolds number
Sc_b		Schmidt number
Δt_p	[s]	particle time step
V,u	[m/s]	velocity

u_i'	[m/s]	fluctuating velocity
Greek letters		
α		phase volume fraction
φ		particle volume fraction
Γ_k	[kg/m^3.s]	Exchanged mass
$\dot{\gamma}$	[1/s]	shear rate
κ	[m^2/s^2]	turbulent kinetic energy
μ	[Pa.s]	viscosity
μ_t	[Pa.s]	turbulent viscosity
Ω	[1/s]	relative particle-liquid angular velocity
ρ	[kg/m^3]	density
σ	[N/m]	surface tension
$\Im_k$, $\Im_k^t$	[Pa]	laminar and turbulent shear stress
ζ_i		Gaussian white noise random number
ξ		random number
Subscript		
k		continues phase
l		liquid
m		mixture
v		vapour
p		particle
sat		saturation
W,s		wall, surface

You and Kim [9] showed that heat transfer coefficient remained nearly unchanged for alumina nanofluid on a flat plate in pool boiling at saturation temperature 60oC. While critical heat flux was found abnormally increased up to 200%. Ham and Cho [10] studied the effects of various parameters on heat transfer, bubble departure frequency, and diameter, waiting time ratio and nucleate site density. They used previous correlations from literature with considering the important impact of surface roughness induced by nanoparticles coating. In addition, variation in contact angle was found as small as 10^o up to the contact angle for pure water on a clean surface as 79^o.

Literature review shows that there are many phenomena involved in pool boiling with solid particles and further theoretical aspects are needed to be investigated regarding particle migration and deposition. Additionally, experimental observations have revealed that non-homogenous distribution of particles inside the medium seems unavoidable, and especially close to the wall boundaries. Accordingly, using the discrete model to track the particles in the Lagrangian frame can provide higher accuracy in prediction. In this study, pool boiling of nanofluid on a cylindrical geometry is simulated by the Eulerian two-phase model. Then, alumina particles are injected into the domain and tracked. Some of the particles leave the domain and a small proportion will deposit on the wall. Local thermo-physical properties of nanofluid are obtained from the non-uniform distribution of particles in the fluid. Eventually, the results will be compared to experimental measurements for the aim of validation and further discussion will be conducted. In addition, the further prediction is conducted for a tube-bundle in pool boiling.

NUMERICAL METHOD AND GOVERNING EQUATIONS

In this model, each phase is treated as a continuum and flow equations are solved in Eulerian manner. The interphase interactions occur at the interface of two phases and appear in each individual equation. The exchange of mass between phases are included in mass balance equation, and associated momentum and energy are added to force and heat transfer balance equations. The fundamental governing equations are as follows [11]:

$$\frac{\partial}{\partial t}(\alpha_k\rho_k)+\nabla.(\alpha_k\rho_k V_k)=\Gamma_k \tag{1}$$

$$\begin{aligned}\frac{\partial}{\partial t}(\alpha_k\rho_k V_k)+\nabla.(\alpha_k\rho_k V_k V_k)&=-\alpha_k\nabla P+\nabla.\left\{\alpha_k\left[\Im_k+\Im_k^t\right]\right\}+\alpha_k\rho_k g_i+M_k\\&+(F_{drag}+F_{lift}+F_{dispersion}+F_{lubrication}+F_{virtual})_k\end{aligned} \tag{2}$$

$$\begin{aligned}\frac{\partial}{\partial t}(\alpha_k\rho_k h_k)+\nabla.(\alpha_k\rho_k V_k h_k)&=\alpha_k\frac{DP}{Dt}+\nabla.\left(q_k+q_k^t\right)\\&+E_k+\alpha_k\left(\Im_k+\Im_k^t\right):V_k\end{aligned} \tag{3}$$

where Γ_k , $\Im_k$, $\Im_k^t$, M_k , q_k , q_k^t and are exchanged mass between phases, laminar shear stress, turbulent shear stress, momentum induced by mass exchanged, laminar and turbulent heat flux and exchanged heat transfer due to mass transfer and between phases, respectively. The interaction forces at the interface consist of drag, lift, turbulent dispersion, wall lubrication, and virtual mass.

Drag force by Clift et al. [12] and Lift force by Tomiyama [13]

$$F_{drag}=\frac{1}{8}A_i\frac{C_D\,Re\,\mu_k}{d_v}|V_l-V_v|(V_l-V_v) \tag{4}$$

$$F_{lift}=C_L\alpha_k\rho_k(V_l-V_v)\times(\nabla\times V_k) \tag{5}$$

The drag coefficient is defined as follows:

$$C_D=max\left[min\left(C_{D_{ellipse}},C_{D_{cap}}\right),C_{D_{Sphere}}\right] \tag{6}$$

$$\begin{cases}C_{D_{Sphere}}=\begin{cases}\dfrac{24}{Re} & Re\le 0.01\\ 24\dfrac{\left(1+0.15\,Re^{0.687}\right)}{Re} & Re>0.01\end{cases}\\ C_{D_{cap}}=\dfrac{8}{3};C_{D_{ellips}}=\dfrac{4}{3}\dfrac{gd^l}{U_t^2}\dfrac{(\rho_k-\rho_l)}{\rho_l}\end{cases} \tag{7}$$

$$\begin{cases}Re=\dfrac{\rho_k|V_l-V_v|d^l}{\mu^k};\ U_t=\dfrac{\mu_k}{\rho_k d_v}Mo^{-0.149}(J-0.857)\\ Mo=\dfrac{\left(\mu^k\right)^4 g(\rho_l-\rho_v)}{(\rho_k)^2\sigma^3}\\ J=\begin{cases}0.94H^{0.757} & 2<H\le 59.3\\ 3.42H^{0.441} & H>59.3\end{cases};\ H=\dfrac{4}{3}Eo\,Mo^{-0.149}\left(\dfrac{\mu_k}{0.0009}\right)^{-0.14}\\ Eo=\dfrac{g(\rho_l-\rho_v)(d_v)^2}{\sigma}\end{cases} \tag{8}$$

Wall lubrication force, Turbulence dispersion and Virtual mass force:

$$F_{lubrication} = C_w \rho_k \alpha_v \left| V_l - V_v \right|^2 n_w \tag{9}$$

$$F_{dispersion} = C_D \frac{\mu_k^t}{\rho_k Sc_b} \left(\frac{\nabla \alpha_l}{\alpha_l} - \frac{\nabla \alpha_v}{\alpha_v} \right) \tag{10}$$

$$F_{virtual} = 0.5 \alpha_k \rho_k \left(\frac{DV_l}{Dt} - \frac{DV_v}{Dt} \right) \tag{11}$$

It can be assumed that mass transfer happens in two different locations, near the wall, and inside the domain. The one in the domain takes place at the interfacial area for both liquid and vapour as follows:

$$\dot{m} = \frac{q_l + q_v}{h_{lv}} \tag{12}$$

$$q_l = \frac{k_l Nu_l}{d_l} \left(T_{sat} - T_l \right); \; q_v = \frac{\alpha_v \rho_v c_{p_v}}{\delta t} \left(T_{sat} - T_v \right) \tag{13}$$

h_{lv}, T_{sat} and δt denote the latent heat of evaporation, saturation temperature, and time scale, respectively. The mass transfer near the wall is assumed to be a part of RPI model.

Evaporative heat flux, convective heat flux, and quenching heat flux:

$$q_e = \frac{\pi}{6} d_W^3 N_W \rho_v h_{lv} \tag{14}$$

$$q_c = h_C \left(T_w - T_l \right) (1 - A_b) \tag{15}$$

$$q_q = C_{qw} \frac{2k_l}{\sqrt{\pi \lambda_l T_b}} \left(T_W - T_l \right) \tag{16}$$

$$T_b = \sqrt{\frac{3\rho_l d_W}{4g\left(\rho_l - \rho_v\right)}} \tag{17}$$

Mass change at the vicinity of the wall:

$$\dot{m} = \frac{q_e}{h_{lv} + c_{p_l} \left(T_{sat} - T_l \right)} \tag{18}$$

DISCRETE MODELLING OF PARTICLES

Particles are tracked in the Lagrangian frame and a set of flow equations are iteratively solved in this model. Hence, a finite number of particles are tracked in each time step as a representative of other particles. The Newton's equation of force balance in the Lagrangian frame for nanoparticles is written in details as follows:

$$m_p \frac{du_p}{dt_p} = F_{drag} + m_p \frac{\vec{g}(\rho_p - \rho_c)}{\rho_p} + F_{lift} + F_{Magnus} + F_{thermo} + F_B \tag{19}$$

The interaction forces are as follows:

$$F_{drag} = \frac{m_p}{\tau} \frac{C_D Re_p}{24 C_c} \left(V_l - u_p \right) \tag{20}$$

$$F_{lift} = 20.3 \mu_l d_p^2 (V_l - u_p) \sqrt{\frac{\dot{\gamma} \rho_l}{\mu_l}} \, \mathrm{sgn}(\dot{\gamma}) \tag{21}$$

$$F_{Magnus} = \frac{1}{2} A_p C_{ML} \rho_c \frac{\left| V_l - u_p \right|}{\left| \Omega \right|} \left[\left(V_l - u_p \right) \times \Omega \right] \tag{22}$$

$$F_{thermo} = -D_T \frac{\nabla T}{T} \tag{23}$$

$$F_B = \zeta_i \sqrt{\frac{6\pi d_p \mu_l K_B T}{\Delta t_p}} \tag{24}$$

The effects of fluctuating velocity on particles trajectory can be seen via using discrete random walk model developed by Bayazit [14]. The fluctuating velocity of an eddy is presented as:

$$u_i' = \xi \sqrt{\overline{u_i'^2}} \tag{25}$$

where ξ is the randomly distributed number from Gaussian pdf and is the root mean square of fluctuating velocity, and as the turbulent kinetic energy. The interaction between the eddy and the particle occurs during the minimum of two characteristic times, the lifetime of the eddy and particle eddy crossing time. At the end of the period, a new location for the particle is calculated. It is noted that random walk model is essential to be considered in particles calculation, specifically regarding the possibility of sedimentation.

Thermophysical properties of liquid are noticeably affected by the presence of particles. Therefore, updated mixture properties are required to be implemented. Due to non-uniform distribution of nanoparticles solved by discrete model, the mixture properties are required to be described in terms of local concentration.

$$\rho_m = \sum_{k=1}^{2} \varphi_k \rho_k \tag{26}$$

$$c_{P_m} = \frac{\sum_{k=1}^{2} \varphi_k \rho_k c_{P_k}}{\rho_m} \tag{27}$$

$$k_m / k_l = 1 + 1.0112\varphi + 2.4375\varphi \left(\frac{47 \times 10^{-9}}{d_p} \right) - 0.0248\varphi \left(\frac{k_p}{0.613} \right) \tag{28}$$

$$\mu_m / \mu_l = \frac{1}{\left[1 - 34.87 \left(d_p / 0.3 \times 10^{-10} \right)^{-0.3} \varphi^{1.03} \right]} \tag{29}$$

Nanoparticles are tracked inside the computational domain and the final distribution of volume fraction provides the mixture properties. The properties are replaced with liquid properties to introduce the impacts of nanoparticles on the flow.

The geometry studies here is a two-dimensional cylinder with 20 mm diameter in a saturated medium. The cylinder is assumed to be in a largely saturated medium with the mixture of alumina particles of 38 nm and distilled water. For the comparison purposes, the experimental work conducted by Das et al. [15] is taken into account. At the next step, a tube bundle is simulated with alumina nanofluid in pool boiling with four tubes vertically oriented. The tube diameter and gap between the tubes are 20 mm and 10 mm, respectively.

MODEL DISCRIPTION

Various types of meshes are generated and tested based on validity of both boiling and discrete models. Since realizable k-ε was chosen as turbulence model, fine mesh was created around the wall of the cylinder to reach y+ less than 1 for enhanced wall treatment. Eulerian-Eulerian accompanied by nucleate boiling approach was employed to simulate multiphase model in the computational domain, while discrete model was used to track the suspended particles. The geometries and generated mesh are illustrated in figure 1. Ansys Fluent is used to iteratively solve the differential equations. Constant heat flux is assumed on each cylinder and pressure boundary conditions are applied at the bottom and top of the model.

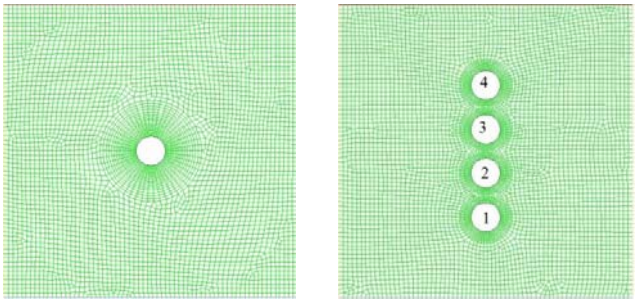

a) b)

Figure 1. Schematic of the geometry considered for nanofluid pool boiling

TRENDS AND RESULTS

The accuracy of the simulated model is shown in figure 2. The error bars are based on the uncertainty value for superheat temperature by Das et al. [15], which is 4%. The simulation results are in good agreement with experiments at lower heat flux and in the range of uncertainty. Although, the findings are still in less than 8% of the measured values at higher heat flux, which can be acceptable for predictions in this range of heat flux. Since the results are now validated, the particles migration and further simulations for tube bundle can be presented.

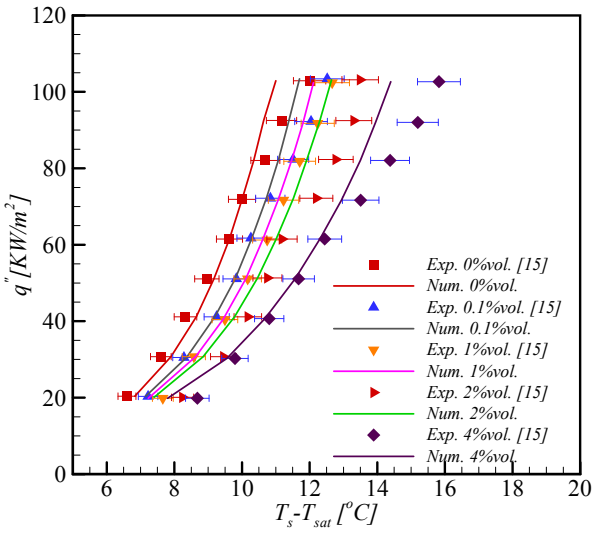

Figure 2. Superheat temperature on the wall of a horizontal cylinder in an alumina nanofluid medium

As previously mentioned, sedimentation of the particles on the wall plays a critical role in bubble formation and liquid surface tension. Due to the sophisticated phenomenon of pool boiling near to the heated wall, only an estimation of particles deposition is presented in figure 3 and its precise contribution on the wall roughness and bubble departure frequency require further investigation. A comparison between the effects of nanoparticles volume fraction and wall heat flux on particles deposition reveals that there can be conditions that the deposition reaches the maximum value and then drops. It occurs somewhere between 0.1% vol. to 1% for all introduced heat flux values. Up to almost 50 KW/m^2, increasing heat flux has shown positive impacts on particles sedimentation and the trends become steady after volume fraction above 2% vol. On the other hand, the trend is completely contrasting when heat flux goes beyond 50 KW/m^2. The reduction in particles deposition in these cases can be referred to the stronger convective flows induced by pool boiling at higher heat flux.

The simulation results of a four-tube bundle with nanofluid in pool boiling are presented in this section. Both superheat temperature (the difference between heated wall temperature and saturation temperature) and heat transfer coefficient on each surface of the tube numbered as one to four are shown in figure 4 and figure 5. It is observed that both the tubes at the middle, namely 2nd and 3rd tubes, have indicated similar trend and values in pool boiling features. Maximum superheat temperature occurs on the bottom tube in all cases. Also, superheat temperature is enhanced on the all tubes with an increase in particles concentration. Evidently, any rise in heat flux on the heated wall develops superheat temperature sharply. On the other hand, the deterioration in heat transfer coefficient by adding particles concentration can be seen in figure 5. When only pure water is used in pool boiling case, as in figure 5a, the difference between heat transfers on tubes is small, while the difference starts growing with the increase in particles concentration. It comes from the fact that the presence of

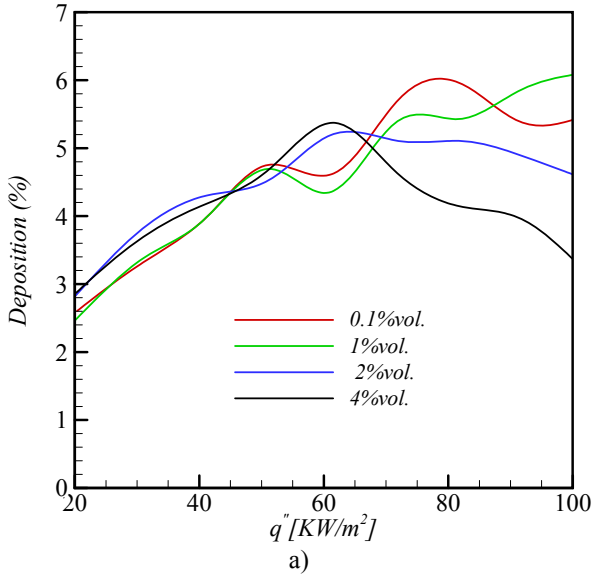

a)

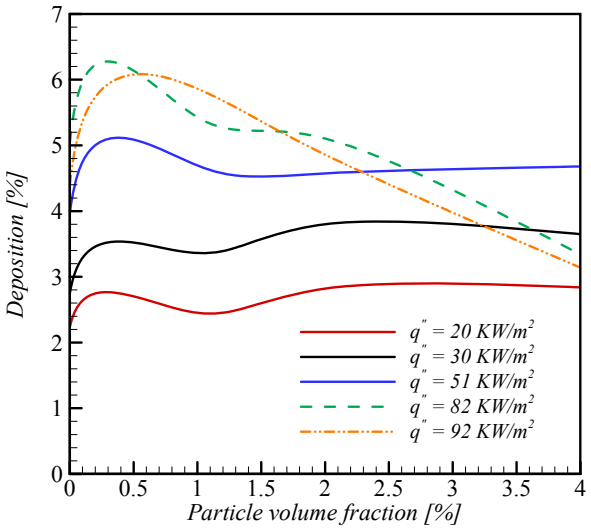

b)

Figure 3. Deposition of the alumina nanoparticles on the surface of a horizontal cylinder

nanoparticles cannot only change the properties of the mixture, it also has effects on the surface of the tubes by considering deposition. Although, heat transfer coefficient develops by expanding heat flux, but the value is always minimum on the bottom tube. One of the reason can come from the presence of stronger flow on the top tube. Flow begins forming on the bottom tube and gradually grows to the top tube. Therefore, weaker fluid flow can be expected around the bottom tube.

CONCLUSION

Heat transfer features and the percentage of deposition of nanoparticles on heated walls were numerically investigated in a pool boiling flow in a single tube and four-tube bundle. The Eulerian-Eulerian multiphase approach was employed to model pool boiling and the Lagrangian frame was used to track particles during boiling on the surface. Consequently, the outcomes of the Lagrangian frame were utilised to extract the local properties of fluid. At the first step, the results of the simulations were compared to and validated with experimental measurements for alumina nanofluid on a heated cylinder in two-dimension. Then, a tube bundle consisting of four tubes on top of each other was simulated and the results for heat transfer and particles deposition were presented. The trend for heat transfer and particles sedimentation was found the same for both tubes at the middle. Heat transfer coefficient reached its maximum value on the top tube and minimum on the bottom one.

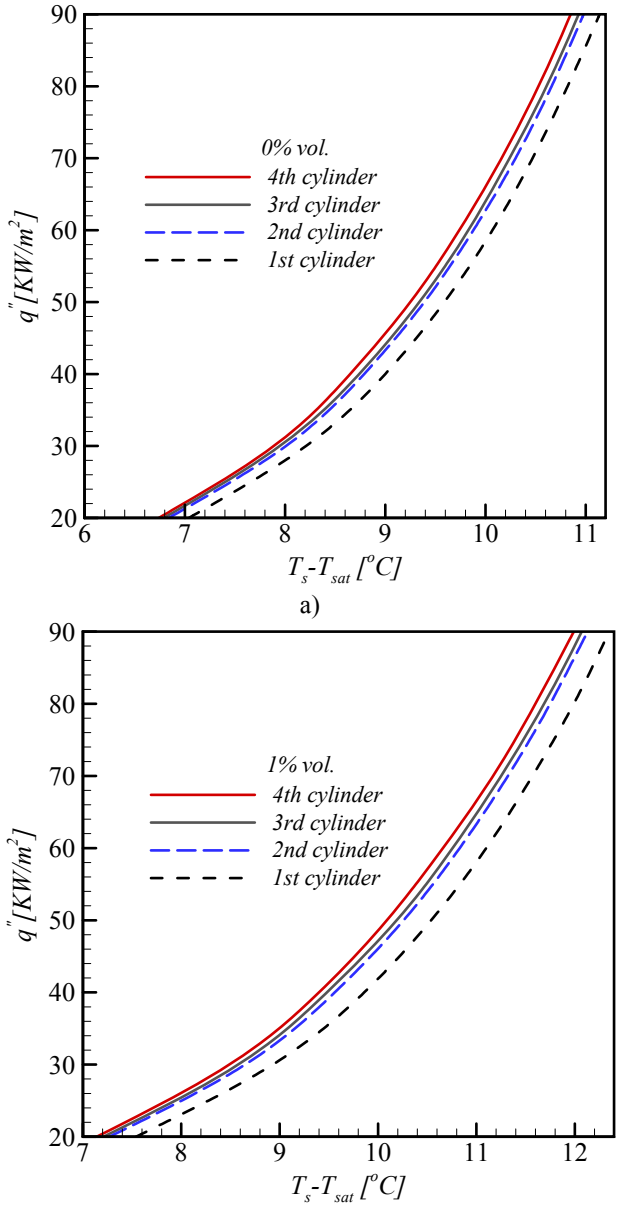

a)

b)

Figure 4. Water and alumina nanofluid pool boiling superheat temperature on the surface of a tube bundle of four horizontal cylinders. a) pure water b) alumina nanofluid 1% vol.

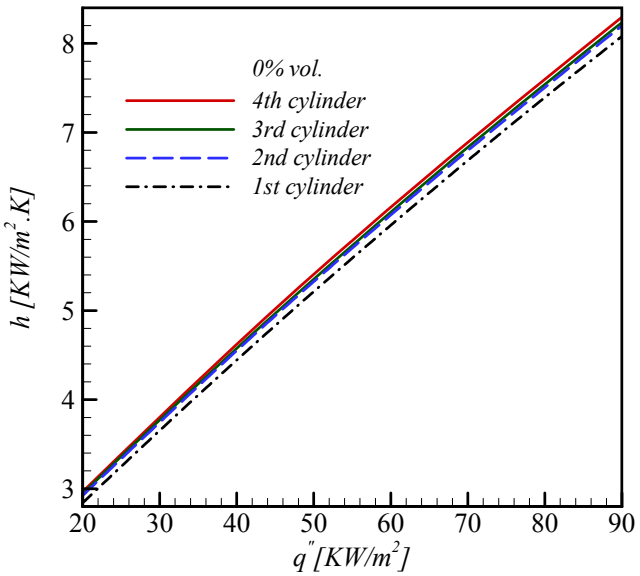

a)

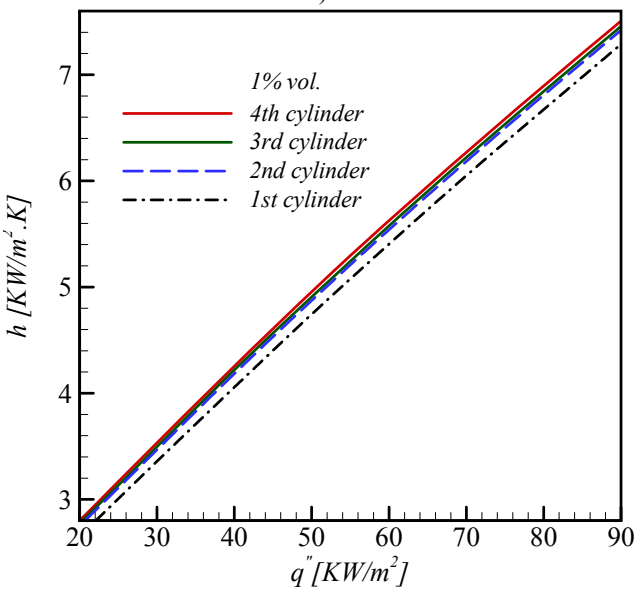

b)

Figure 5. Heat transfer coefficient on the surfaces of cylinders in a four-tube bundle with water and alumina nanofluid in pool boiling. a) pure water b) alumina nanofluid 1% vol.

REFERENCES

[1] Koo, J., Kleinstreuer, C., Laminar nanofluid flow in microheat-sinks, *International Journal of Heat and Mass Transfer*, Vol. 48, 2005, pp. 2652–2661.

[2] Prasher, R., Phelan, P.E., Bhattacharya, P., Effect of aggregation kinetics on the thermal conductivity of nanoscale colloidal solutions (nanofluid), *Nano Letter*. Vol. 6, 2006, pp. 1529–1534.

[3] Utomo, A.T., Haghighi, E.B., Zavareh, A.I.T., Ghanbarpour geravi, M., Poth, H., Khodabandeh, R., Palm, B., Pacek, A.W., The effect of nanoparticles on laminar heat transfer in a horizontal tube, *International Journal of Heat and Mass Transfer*, Vol. 69, 2014, pp. 77–91.

[4] Liu, D., Yu, L., Single-phase thermal transport of nanofluids in a minichannel, *Journal of Heat Transfer* Vol 133, 2011, pp. 31009.

[5] Duangthongsuk, W., Wongwises, S., An experimental study on the heat transfer performance and pressure drop of TiO2-water nanofluids flowing under a turbulent flow regime, *International Journal of Heat and Mass Transfer*, Vol. 53, 2010, pp. 334–344.

[6] He, Y., Jin, Y., Chen, H., Ding, Y., Cang, D., Lu, H., Heat transfer and flow behaviour of aqueous suspensions of TiO 2 nanoparticles (nanofluids) flowing upward through a vertical pipe, *International Journal of Heat and Mass Transfer*, Vol. 50, 2007, pp. 2272–2281.

[7] Bang, I.C., Heung Chang, S., Boiling heat transfer performance and phenomena of Al2O3–water nano-fluids from a plain surface in a pool, *International Journal of Heat and Mass Transfer*, Vol. 48, 2005, pp. 2407–2419.

[8] Shoghl, S.N., Bahrami, M., Jamialahmadi, M., The boiling performance of ZnO, a-Al2O3 and MWCNTs/water nanofluids: An experimental study, *Experimental Thermal and Fluid Science*, Vol. 80, 2017, pp. 27–39.

[9] You, S.M., Kim, J.H., Kim, K.H., Effect of nanoparticles on critical heat flux of water in pool boiling heat transfer, *Applied Physics Letter*, Vol 83, 2003, pp. 3374–3376.

[10] Ham, J. Cho, H., Theoretical analysis of pool boiling characteristics of Al_2O_3 nanofluid according to volume concentration and nanoparticle size, *Applied Thermal Engineering*, Vol 108, 2016, pp. 158–171.

[11] Ishii, M., Hibiki, T., Thermo-fluid dynamics of two-phase flow, Springer Science & Business Media, 2010.

[12] Clift, R., Grace, J.R., Weber, M.E., Bubbles, drops, and particles, Courier Corporation, 2005.

[13] Tomiyama, A., Struggle with computational bubble dynamics, *Multiphase Science Technology*, Vol 10, 1998, pp. 369–405.

[14] Bayazit, M., Random Walk Model For Motion Of A Solid Particle In Turbulent Open-Channel Flow, Journal of Hydraulic Research, Vol 10, 1972, pp. 1–14.

[15] Das, S.K., Kumar, R., Moreno, G., Yoo, J., You, S.M., Pool boiling characteristics of low concentration nanofluids, *International Journal of Heat and Mass Transfer, Vol* 53, 2010, pp. 972–981.